Correspondence to:
C. Coulon,
cecile.coulon.1@ulaval.ca

Pumping Optimization Under Uncertainty in an Island Freshwater Lens Using a Sharp-Interface Seawater Intrusion Model

Cécile Coulon[1,2,3] , Jean-Michel Lemieux[1,2,3] , Alexandre Pryet[4], Peter Bayer[5], Nathan L. Young[1,2,3] , and John Molson[1,2,3]

[1]Département de géologie et de génie géologique, Université Laval, Québec, QC, Canada, [2]Centre québécois de recherche sur l'eau, Québec, QC, Canada, [3]Centre d'études nordiques, Université Laval, Québec, QC, Canada, [4]EA 4592 Géoressources et Environnement, Bordeaux INP and University Bordeaux Montaigne, Pessac, France, [5]Department of Applied Geology, Martin Luther University of Halle-Wittenberg, Halle, Germany

Abstract Pumping optimization under uncertainty is a powerful approach for the management of groundwater resources, and its implementation would be valuable in island aquifers where freshwater lenses are affected by seawater intrusion. Sharp-interface numerical models are especially well suited for the task as they offer fast simulation times, but to date they have not been used because of a lack of guidelines and due to the specific challenges associated with this approach. This study presents a methodology for pumping optimization under uncertainty for island freshwater lenses using a sharp-interface model (MODFLOW-SWI2) and demonstrates it for a real case (Magdalen Islands, Quebec, Canada). The total pumping in a well field was maximized while avoiding well salinization due to upconing. To do so, the sharp interface simulated below the pumping wells was corrected successively for cell-to-well upconing and for dispersion. Pumping optimization under uncertainty was then conducted using PESTPP-OPT, considering parameter and observation uncertainty, and was repeated for 23 reliability levels to illustrate a large range of risk-averse, tolerant and neutral stances. The maximum pumping was obtained as a function of risk of well salinization. This approach enabled quantification of the tradeoffs between pumping and risk, allocation of pumping amongst wells, and an examination of the ability of the well field to meet the water demand while maintaining an acceptable level of risk. Ultimately, this framework allows groundwater managers to select the final pumping scenario themselves, depending on their attitude toward risk.

Plain Language Summary Fresh groundwater is an important source of drinking water in island environments, but its proximity to seawater makes it vulnerable to salinization. In these areas, fresh groundwater is often contained in a lens that overlies saline groundwater. Pumping within the freshwater lens to extract drinking water causes saltwater to migrate toward the pumping well, a phenomenon called saltwater upconing. As a result, water managers need to balance meeting the water demands of the local community with avoiding saltwater contamination of local drinking water supplies. Computer simulations of groundwater flow are commonly used to inform groundwater management decisions, but the uncertainties associated with these simulations are usually neglected, often resulting in the consideration of a single management solution. To improve water management strategies in freshwater lenses, we developed a new technique to evaluate the maximum amount of freshwater that can be safely pumped from the lens while recognizing the impact of simulation uncertainties on management solutions. Multiple pumping rate scenarios were generated, each associated with a different risk of well contamination between 0% and 100%. This method allows local water managers to then choose their preferred pumping scenario depending on the level of risk that they consider to be acceptable.

1. Introduction

Island groundwater resources often form freshwater lenses overlying saline groundwater. When water is withdrawn from a freshwater lens by a pumping well, saline groundwater migrates upwards toward the well. This vertical seawater intrusion process, also called saltwater upconing, is a major concern when managing well fields. Freshwater lenses of island aquifers have been described as being more vulnerable than continental coastal aquifers, since vertical migration distances associated with upconing are shorter than horizontal ones (Jiao &

Post, 2019). They have also been described as requiring particular attention when solving coastal groundwater management problems (Ketabchi & Ataie-Ashtiani, 2015). In these environments, determining sustainable yields using pumping optimization under uncertainty is valuable, since optimization methods provide transparent and optimal solutions to management problems, and since quantifying how modeling uncertainties affect management solutions is crucial for informed decision-making (Horne et al., 2016; White et al., 2018).

Sharp-interface (SI) numerical models assume that freshwater and seawater are immiscible and separated by a sharp boundary, whereas advective-dispersive-based variable-density (VD) models explicitly simulate mixing between freshwater and seawater by solving both the variable-density groundwater flow equation and the advection-dispersion equation for solute transport. SI models are most useful for simulating regional-scale seawater intrusion, where dispersion can be neglected. In island aquifers, SI models are commonly used to assess the extent of freshwater lenses and establish water budgets (Izuka et al., 2021; Lotti et al., 2021; Shuler & Mariner, 2020), while their fast simulation times also facilitate parameter estimation and quantification of predictive uncertainty (Coulon et al., 2021). Because of their rapid simulation times, SI models are widely used to optimize pumping rates in continental coastal aquifers, which are faced with the threat of lateral seawater intrusion (Kopsiaftis et al., 2019). However, they have not yet been used for pumping optimization in island freshwater lenses where vertical seawater intrusion (i.e., upconing) is a major risk. This is because pumping and upconing lead to increased dispersion and a widening of the transition zone below the pumping wells, which violates the sharp interface assumption.

Furthermore, conducting pumping optimization under uncertainty is rare both in coastal and island aquifers because of its high computational cost. Previous work on optimized saltwater intrusion management has been mainly dedicated to deterministic problems (Ketabchi & Ataie-Ashtiani, 2015). Predictive uncertainty due to insufficient knowledge of recharge, hydraulic or transport parameters was included by training surrogate or meta-models (e.g., Lal & Datta, 2019; Rajabi & Ketabchi, 2017). While surrogate models are a popular choice to replace computationally demanding physically based models, in practice they are limited because of the considerable effort needed for training surrogates, the need to verify optimized solutions with physically based models and the significant expertise that is needed for their robust application. Many optimizations under uncertainty have remained limited to hypothetical or simplified real-world cases (Mostafaei-Avandari & Ketabchi, 2020) and guidance is lacking for their implementation in real-world cases (Ketabchi & Ataie-Ashtiani, 2015). The objective of this paper is therefore to provide a methodology for pumping optimization under uncertainty in a freshwater lens, using a SI model. The approach is then demonstrated for the Magdalen Islands (Quebec, Canada).

A SI numerical model is first developed for an island freshwater lens, using MODFLOW-SWI2 (Bakker et al., 2013). After postprocessing the interface simulated by SWI2 under pumping wells, pumping optimization under uncertainty is conducted using PESTPP-OPT (White et al., 2018) for a wide range of risk-averse, tolerant or neutral stances, to understand how modeling uncertainties and attitude toward risk affect optimal management strategies. This workflow uses widely available hydrogeological software and all Python scripts are available to promote transparency and reproducibility.

2. Study Area

The Magdalen Islands (Quebec, Canada) are an archipelago in the Gulf of Saint-Lawrence in which fresh groundwater is the sole water supply for its 12,000 permanent inhabitants and its 70,000 yearly visitors. As the water resources are under pressure due to climate change, hydrocarbon exploration and intense tourism, a groundwater knowledge acquisition project was launched (a) to assess groundwater resources at the island scale and (b) to provide sustainable groundwater pumping scenarios. On Grande Entrée Island, which is the most vulnerable island to seawater intrusion because of its shallow saline groundwater, the development of a SI model, parameter estimation and linear uncertainty analysis allowed for an assessment of the extent of the freshwater lens (Coulon et al., 2021). In this paper, pumping optimization under uncertainty is conducted to provide decision-support for the management of municipal groundwater pumping.

Grande Entrée Island has an area of 8.5 km^2, with low-lying topography and negligible surface water. The main aquifer formation is a highly permeable Permian sandstone with an estimated thickness of 300 m (Brisebois, 1981). Sand dunes are found locally and low-permeability glacial sediments fill a paleovalley in the middle of the island (Figure 1). Recharge has been evaluated at 559 mm/year, representing approximately 54% of the annual
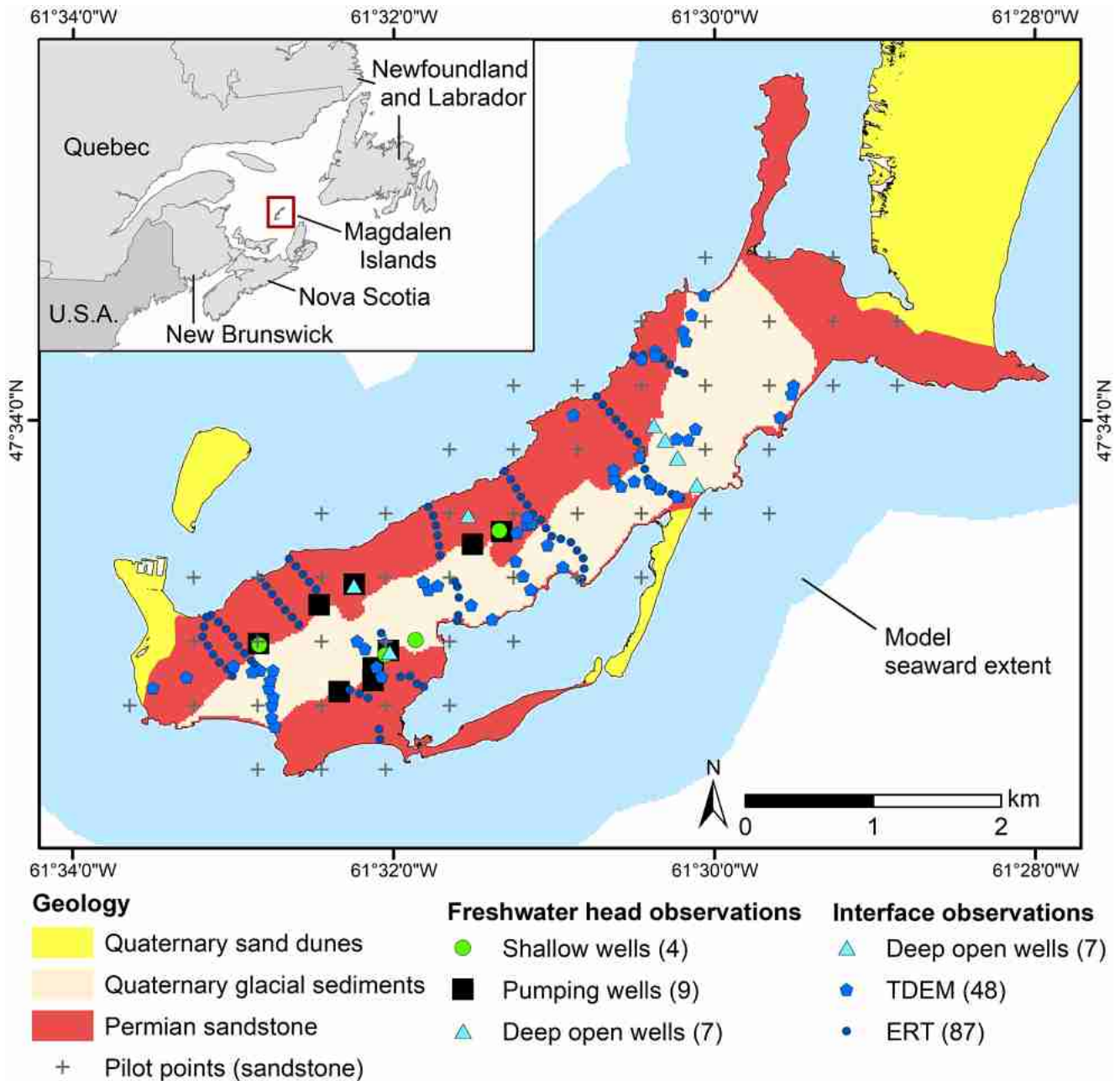
Figure 1. Map of Grande Entrée Island with seaward extent and geological formations, locations of pilot points, pumping wells, and model observations. Domestic wells are not shown. Modified from Coulon et al. (2021).

precipitation (Lemieux et al., 2022). The reader is referred to Coulon et al. (2021) for more details on the study area. Nine municipal wells have been pumping water from the freshwater lens since 2013, with pumping rates and water levels being recorded since mid-2014. Between 2014 and 2019, average pumping rates at these wells were below 25 m^3/day, for a total pumping rate in the well field close to the 110 m^3/day water demand (Lemieux et al., 2022). Apart from one screened well, all wells are open boreholes which do not contain casing or screening (aside from a casing near the ground surface to prevent erosion or cave-in). The freshwater-saltwater transition zone can be observed in 7 deep, open observation wells present in the study area (Figure 1). The transition zone is relatively narrow (8 m on average) compared to the estimated aquifer thickness (around 300 m), suggesting that hydrodynamic dispersion is less important than advection, and it is relatively shallow (around 45 m below local sea level) relative to well bottom elevations (between 11 and 32 m below local sea level), indicating that

Table 1
Posterior Parameter Distributions Described by the Mean and the 95% Confidence Interval (i.e., the Mean ± 2 Standard Deviations)

Parameter	Mean	95% confidence interval
$K_{sand\ dunes}$ (m/s)	5×10^{-4}	5×10^{-6}–5×10^{-2}
$K_{sandstones}$ (m/s) (offshore)	3×10^{-4}	4×10^{-5}–2×10^{-3}
$K_{sandstones}$ (m/s) (52 pilot points)	2×10^{-4}	–
$K_{glacial\ sediments}$ (m/s)	1×10^{-4}	3×10^{-6}–3×10^{-3}
K_{seabed} (m/s)	9×10^{-6}	5×10^{-6}–2×10^{-5}
Recharge (mm/yr)	547	401–693
Transverse vertical dispersivity α_T (m)	6×10^{-3}	3×10^{-4}–1×10^{-1}

Note. Distributions were assumed log-normal or normal for recharge. The average value of the pilot point hydraulic conductivities is reported; 95% confidence intervals are not reported since they depend on pilot point location. Modified from Coulon et al. (2021).

the municipal pumping wells are under threat of upconing. For the rest of the paper, the term "pumping wells" will be used to refer to the municipal pumping wells only (excluding domestic wells).

3. Methods

3.1. Numerical Model

The numerical model, the parameter estimation procedure and results are described in detail in Coulon et al. (2021). A sharp-interface, 2D-horizontal model with a regular, 20×20 m grid was developed for the island (Figure 1) using the SWI2 package (Bakker et al., 2013) for MODFLOW-2005 (Harbaugh, 2005). SWI2 simulates vertically integrated variable-density groundwater flow using zones of different density separated by sharp interfaces, but does not account for diffusion and mechanical dispersion as in advective-dispersive-based VD models. The single model layer contained constant-density freshwater and seawater zones separated by a sharp interface representing the 50% seawater salinity (total dissolved solids or TDS) contour (i.e., a mix of 50% seawater and 50% freshwater). Pumping wells were simulated using the revised multinode well package (MNW2 package, Konikow et al., 2009), in order to assimilate water level observations during parameter estimation (Coulon et al., 2021) and to correct the simulated interface for cell-to-well upconing during pumping optimization (Section 3.2.2). The heterogeneous hydraulic conductivity field was parameterized by combining zones of constant hydraulic conductivity and pilot points (Doherty, 2003). Homogeneous effective porosity and specific yield values were implemented for all cells, and a uniform recharge rate was implemented on land cells.

Regularized parameter estimation was carried out using PEST_HP (Doherty, 2020). The model was calibrated under steady-state conditions with boundary conditions representative of the period 2014–2019. Fifty-eight model parameters were adjusted, including 56 hydraulic conductivities, surface recharge and transverse dispersivity. The latter was used as a correction factor for the sharp interface (Coulon et al., 2021), since for steady-state flow conditions with dominantly horizontal flow, the development of a transition zone is mainly controlled by transverse vertical dispersion (Jiao & Post, 2019). Parameter estimation was constrained by 162 observations, including freshwater head observations extracted from shallow wells, deep open wells and pumping wells, as well as interface observations (i.e., elevations of the freshwater-seawater interface) derived from electrical conductivity profiles at deep open wells, time-domain electromagnetic (TDEM) and electrical resistivity tomography (ERT) surveys (Figure 1). Parameter estimation required 1,847 simulations, which took a total of 10.5 hr using 70 cores at 2.1 GHz. The posterior parameter set was used throughout the rest of the study (Table 1), since it represents the minimum error variance parameter set resulting in minimum error variance predictions.

The steady-state freshwater lens that would be obtained without pumping was chosen as the initial condition for the pumping optimization (Figure 2). This was achieved by running a long transient simulation (500 years) under the average stresses of the calibration period, but without pumping.

3.2. Postprocessing of the Simulated Interface

3.2.1. Defining Well Salinization

Bakker et al. (2013) demonstrated the use and accuracy of the SWI2 package to simulate upconing below a pumping well, through two examples. In a radial upconing problem, they found that the freshwater-seawater interface simulated by SWI2 closely resembled the 50% seawater salinity contour simulated by the advective-dispersive-based SEAWAT model (Langevin et al., 2008). They also presented an application of SWI2 for the simulation of upconing in an island freshwater lens. While SWI2 simulates the 50%
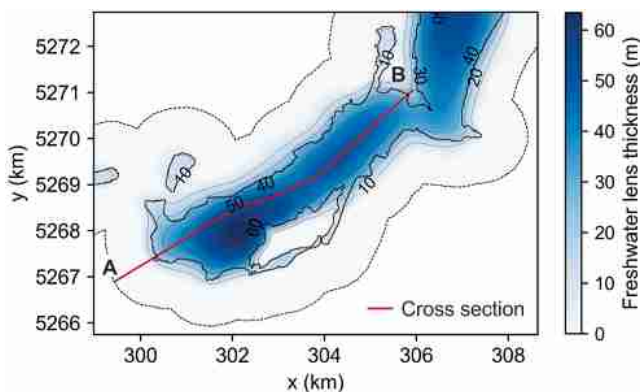

Figure 2. Map of the steady-state freshwater lens under the average stresses of the calibration period, without pumping. This was the initial condition for the pumping optimization. The transect AB corresponds to the cross-section in Figure 11.
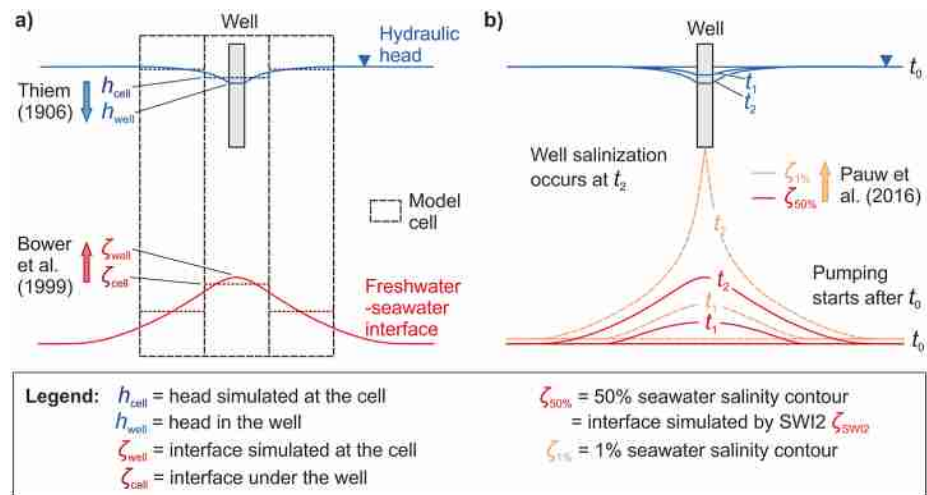
Figure 3. Postprocessing implemented in cells containing pumping wells: (a) correction for cell-to-well upconing and (b) correction for dispersion. Recall that the 1% salinity (TDS) contour is considered representative of 250 mg/L chloride.

seawater salinity (TDS) contour, it is expected that the salinity of the pumped water will increase due to dispersion before this contour reaches the well. In pumped water, a mixing of 1% seawater with freshwater will result in TDS concentrations of about 350 mg/L, equivalent to about 190 mg/L chloride, which is a conservatively low estimate of the 250 mg/L esthetic limit for potable water (WHO, 2003). The 1% figure is also quoted by Jiao and Post (2019). Therefore, this study considered well salinization to occur when the 1% seawater salinity contour ($\zeta_{1\%}$) reached the bottom of the pumping well. In this case, pumped water salinity would not immediately reach 1% seawater, since it depends on mixing effects in the well, and on well length and well diameter. Therefore, this definition was conservative, which was advisable since the consequences of well salinization can be long-lasting and there are no alternative drinking water sources on the island. To obtain $\zeta_{1\%}$ at pumping well locations, two postprocessing steps needed to be implemented successively on the interface simulated by SWI: (a) correction for cell-to-well upconing and (b) correction for dispersion (Figure 3).

3.2.2. Correction for Cell-To-Well Upconing

A first analytical correction was applied to the interface simulated by SWI2, to correct for the difference between upconing in the model cell and upconing directly under the well (or cell-to-well upconing). This step was necessary because finite-difference grids with large cell sizes cannot accurately represent heads and interface elevations under pumping wells with smaller radii. Drawdown and upconing at the well are underestimated as they are averaged across the cell area (Charbeneau, 1995; Dagan, 1995). With the MNW2 package (Konikow et al., 2009), the head simulated at the cell (h_{cell}, in m above local sea level, or masl) was corrected for the difference between cell size and well radius using the Thiem (1906) steady-state flow equation, to obtain the head in the well (h_{well}, in masl). Then, Equation 1 was used to relate cell-to-well drawdown (s, in m) with cell-to-well upconing (Δ, in m):

$$\Delta = \frac{s}{\varepsilon} \tag{1}$$

where s and Δ are defined as:

$$\begin{cases} s = h_{cell} - h_{well} \\ \Delta = \zeta_{well} - \zeta_{cell} \end{cases} \tag{2}$$

and ε is the density ratio between the freshwater and seawater densities ρ_f (1,000 kg/m³) and ρ_s (1,025 kg/m³), respectively:

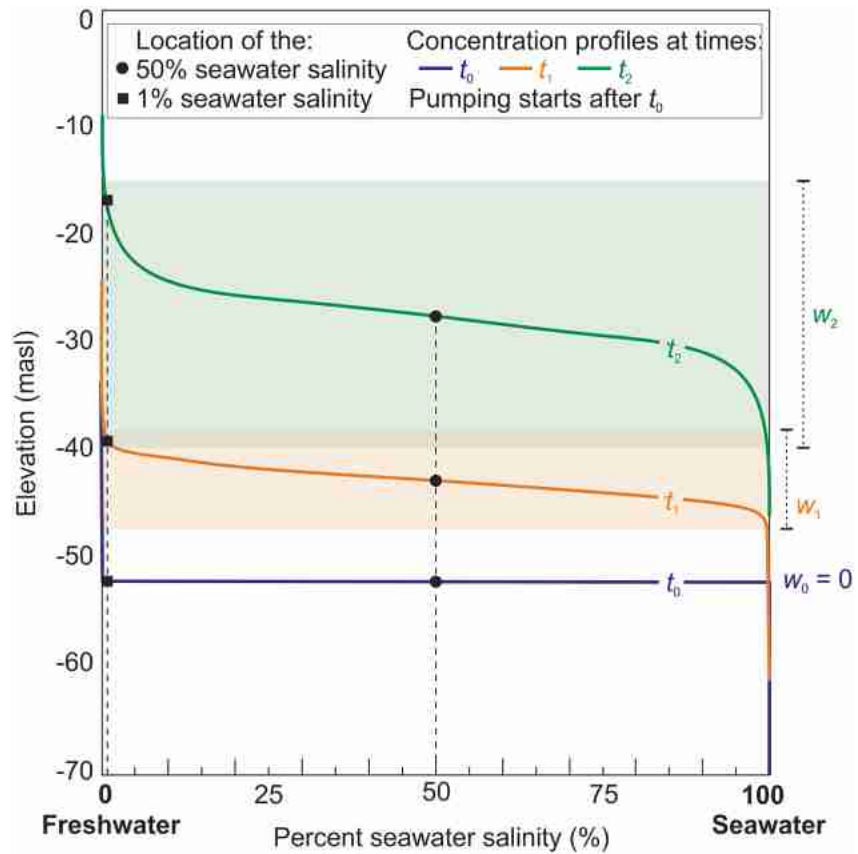$$\varepsilon = \frac{\rho_s - \rho_f}{\rho_f} \tag{3}$$

Figure 4. Schematic widening of the transition zone during pumping when applying the first-order approximation for dispersion (Equation 5). Concentration profiles and corresponding transition zone widths (*w*) are shown at different times, starting from an initially zero transition zone width.

Substituting Equation 2 into Equation 1, the interface elevation simulated at the cell (ζ_{cell}, in masl) could therefore be corrected for cell-to-well upconing, to obtain the interface elevation directly under the well (ζ_{well}, in masl):

$$\zeta_{\text{well}} = \zeta_{\text{cell}} + \frac{h_{\text{cell}} - h_{\text{well}}}{\varepsilon} \tag{4}$$

Equation 1 corresponds to Equation 6 of Bower et al. (1999), which was originally developed to relate the critical rise of the interface under a pumping well to drawdown, in a model with immiscible freshwater and saltwater assuming the Ghyben-Herzberg relation.

3.2.3. Correction for Dispersion

A second analytical correction was applied to the interface simulated by SWI2, to obtain a first-order approximation of dispersion in the transition zone during pumping, and to obtain the elevation of the 1% seawater salinity contour (Figure 4). This analytical equation was originally developed by Bear and Todd (1960), to approximate the concentration distribution in the transition zone following the displacement of an initially sharp interface. They treated upconing as a 1D, upward solute transport process in an infinite and homogeneous domain. It was subsequently superimposed onto SI analytical solutions (Pauw et al., 2016; Schmorak & Mercado, 1969) and SI numerical models (Wirojanagud & Charbeneau, 1985), with modifications to incorporate an initially non-zero transition zone width. Schmorak and Mercado (1969) compared the approach to field observations of upconing and found it was justified as a first approximation of the transition zone, while Wirojanagud and Charbeneau (1985) used it to reduce the prediction error caused by the simplification of physical processes. Pauw et al. (2016) explored the applicability of the approach for a wide range of parameters through comparison with

Table 2
Model Parameters Introduced Into the Correction for Dispersion

Parameter	Mean	95% confidence interval
Initial transition zone width M (m)	8	5–11
Longitudinal dispersivity α_L (m)	3	1–5

Note. Distributions are described by the mean and the 95% confidence interval (normal distributions assumed).

the SEAWAT model, which is further discussed in Section 5.2. With this correction, the elevation of the 1% seawater salinity contour $\zeta_{1\%}$ (masl) could be calculated at any time t using:

$$\zeta_{1\%}(t) = \zeta_{\text{SWI2}}(t) + 2\sqrt{b\,M^2 + \alpha_L|\zeta_{\text{SWI2}}(t) - \zeta_{\text{SWI2 init}}|}\,\text{erfc}^{-1}\left(2\frac{C_{1\%}}{C_s}\right) \quad (5)$$

where ζ_{SWI2} and $\zeta_{\text{SWI2 init}}$ are the interface elevations simulated by SWI2 (i.e., the 50% seawater salinity contour) at time t and the initial state (before pumping), respectively (masl), C_s and $C_{1\%}$ are the concentrations corresponding to pure seawater and 1% seawater (i.e., $0.01 \cdot C_s$), respectively (dimensionless ratio), α_L is the longitudinal dispersivity (m), M is the initial width of the transition zone (m) defined as the 95% confidence interval around the 50% seawater salinity contour (i.e., ± two standard deviations, assuming a Gaussian concentration distribution), and b is a constant defined by:

$$b = \left(\frac{1}{4\,\text{erfc}^{-1}\left(2\frac{C_{2.4\%}}{C_s}\right)}\right)^2 \quad (6)$$

where $C_{2.4\%}$ is the concentration corresponding to 2.4% seawater (i.e., $0.024 \cdot C_s$). ζ_{SWI2} (Equation 5) was substituted by ζ_{well} (Equation 4), while $\zeta_{\text{SWI2 init}}$ did not require correction for cell-to-well upconing since the initial pumping rate was zero (Section 3.1). Equation 5 was derived from Equation 6 in Pauw et al. (2016), and equation derivations for obtaining any x-percent seawater salinity contour are summarized in Appendix A. This approach assumes that mixing in the transition zone is due to longitudinal dispersion, while transverse dispersion and molecular diffusion are neglected. The assumption of homogeneous conditions in this correction was supported by the relative homogeneity of the aquifer formation and was consistent with the absence of vertical hydraulic conductivity variations in the model. The assumption that molecular diffusion was negligible compared to mechanical dispersion was supported by the high hydraulic conductivity of the aquifer and is often assumed in the transition zone (Bear & Todd, 1960). Upconing needed to start in an initially pure freshwater column, therefore pumping optimization started in a steady-state freshwater lens without pumping.

The contribution of parameters α_L and M introduced in Equation 5 was included in the calculation of constraint uncertainty (Section 3.3.3). Their mean values and 95% confidence intervals were estimated assuming Gaussian distributions (Table 2). Values for M were based on transition zone widths extracted from deep observation wells far from the pumping wells (Figure 1). These were assumed to represent the initial transition zone width under "natural" conditions. Values for α_L, for which field data was unavailable, were calculated the following way: (a) the scale of the solute transport problem L was defined, (b) empirical formulas relating L to α_L were applied on minimum, average, and maximum L values, and (c) statistical analyses were carried out on the resulting α_L values. L was defined as the distance between the base of the well and the initial interface elevation simulated by SWI2 (at steady state without pumping), which was 32 m on average. Scaling laws suggested by Neuman (1990) and Xu and Eckstein (1995) were applied (Table 3). The final α_L values introduced in Equation 5 were approximately 2 to 3 orders of magnitude higher than the α_T value used as a general correction factor for the SI model (Section 3.1), which is consistent with published dispersivity ratios used in field-scale advective-dispersive transport modeling (Frind & Germain, 1986; Molson & Frind, 2012).

Table 3
Formulas Relating Solute Transport Scale L to Longitudinal Dispersivity (α_L), for the Minimum, Average and Maximum L Values Computed for the Study Area (L_{min}, L_{mean}, and L_{max}, Respectively)

Reference	Empirical formula α_L (L)	α_L (m) for $L_{min} = 21$ m	α_L (m) for $L_{mean} = 32$ m	α_L (m) for $L_{max} = 48$ m
Xu and Eckstein (1995)	$0.83 \cdot (\log(L))^{2.414}$	1.6	2.2	2.9
Neuman (1990)	$0.017 \cdot (L)^{1.5}$	1.6	3.0	5.6

3.3. Pumping Optimization

3.3.1. Problem Formulation

The objective of the optimization was to maximize the freshwater withdrawals from the pumping wells, while avoiding well salinization due to seawater upconing. In mathematical terms, a single-objective optimization problem was defined:

$$\text{Maximize } \Phi = \sum_{i=1}^{n} Q_i, \quad \text{subject to } \zeta_{1\% i} \leq z_{\text{botm } i} \ (i = 1, ..., n) \tag{7}$$

where Φ is the management objective function (m³/s), n is the number of pumping wells (nine in total), Q_i variables are the pumping rates (withdrawals) applied in each pumping well i (m³/s) or the decision variables of the optimization problem, $\zeta_{1\% \, i}$ is the elevation of the 1% seawater salinity contour under the ith pumping well (masl) and $z_{\text{botm } i}$ is the elevation of the well bottom i (masl). Keeping $\zeta_{1\%}$ below z_{botm} at each pumping well constituted the model-derived optimization constraints. The risk of well salinization due to lateral seawater intrusion was neglected, since the pumping wells were far inland (Figure 1).

Pumping optimization was conducted under steady-state conditions, with average boundary conditions representative of the calibration period (except for pumping rates). Starting from an initial state without pumping (Section 3.1), a long transient simulation was run (200 years), to allow the freshwater lens to reach a new steady state under the Q_i values tested. The respect of the optimization constraints (Equation 7) was examined at the new steady-state condition. Model simulation times were short, averaging 8 min on a laptop computer (1.9 GHz Intel Core i7®).

3.3.2. Sequential Linear Programming

Pumping optimization was conducted using sequential linear programming (SLP) as implemented in the PESTPP-OPT software (White et al., 2018 and references herein). PESTPP-OPT requires (a) an expression of the management objective function as a linear combination of decision variables, (b) an approximately linear relation between decision variables and constraints, and (c) for FOSM-based chance constraints (Section 3.3.3), an approximately linear relation between parameters and constraints. As in the PEST software, model linearization is performed through the computation of constraint sensitivities with a finite-difference scheme. The linear programming problem is then solved using the simplex algorithm (Dantzig et al., 1955). In the implementation of sequential linear programming, which can accommodate a certain level of nonlinearity between decision variables and constraints, the model linearization and simplex algorithm are repeated with the updated values of the decision variables until convergence.

The applicability of PESTPP-OPT was justified since the management objective function was a linear combination of pumping rates (Equation 7) and a nearly linear relation was found between parameters and $\zeta_{1\%}$ values (using the JACTEST utility of PEST; Doherty, 2004) and between pumping rates and $\zeta_{1\%}$ values (Figure 5). Also, starting the optimization from different initial pumping rates yielded the same results, indicating that PESTPP-OPT was effective in finding the global optimum. SLP was implemented since optimization results were slightly improved after the first optimization iteration and because it was numerically efficient. The implementation of PESTPP-OPT was straightforward after having already used a member of the PEST suite to conduct parameter estimation (Section 3.1). Only a few modifications were required to the PEST++ control file and all file processing was handled in Python using the PyEMU library (White et al., 2016).

3.3.3. Optimization Under Uncertainty

Uncertainty in model parameters (aleatory uncertainty) and in observations used to condition these parameters (measurement noise) results in constraint uncertainty. PESTPP-OPT can account for the impact of these uncertainties on optimization results (White et al., 2018). In its FOSM-based chance-constrained programming, constraint standard deviations (σ_{cons}) are evaluated using FOSM (first-order, second-moment) analysis. The optimization problem is then solved using the constraint values shifted by the product of σ_{cons} and the probit function (i.e., the inverse of the cumulative distribution function associated with the standard normal distribution) corresponding to the desired reliability level (Wagner & Gorelick, 1987). Using the terminology from Bear and Cheng (2010), we refer to PESTPP-OPT's "*risk*" values as reliability levels (reliability = 100 · "*risk*"). These represent the probability that the constraints are truly satisfied, considering their uncertainty.
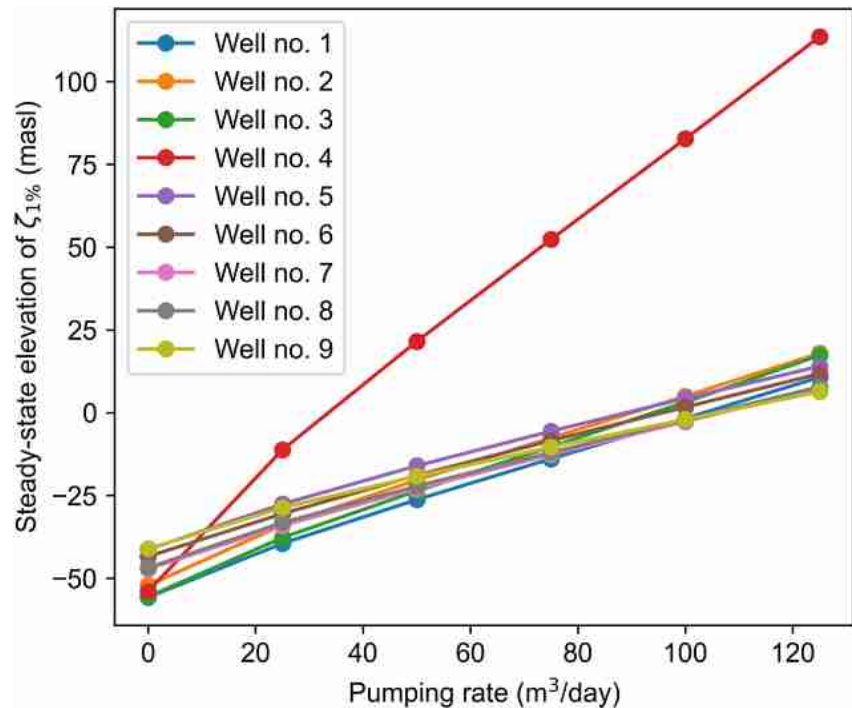
Figure 5. Approximately linear relation between the model-derived constraint $\zeta_{1\%}$ (the 1% seawater salinity contour) and decision variable values (the individual pumping rates).

The optimizations were run with the posterior parameter set and posterior $\zeta_{1\%}$ standard deviations. In the implementation of FOSM-based chance constraints, the 58 parameters adjusted during calibration (Table 1) and parameters M and α_L (Table 2) were considered to be uncertain, as well as the 162 observations in the calibration data set. As a result of the FOSM analysis, all uncertainties were assumed to be Gaussian. The optimization problem was solved repeatedly for a series of 23 reliability levels between 1% and 98%. The reliability level (R) represents the probability of having no well salinization at the end of an optimization (success) and $100 - R$ represents the probability of well salinization (failure). The latter will be referred to as risk of well salinization. A risk-neutral optimization was represented by a 50% reliability level (Figure 6b), while different degrees of risk aversion and tolerance were explored by using higher (Figure 6a) and lower (Figure 6c) reliability levels, respectively. Chance constraints were recalculated at every SLP iteration, since the sensitivity of constraints to parameters could vary
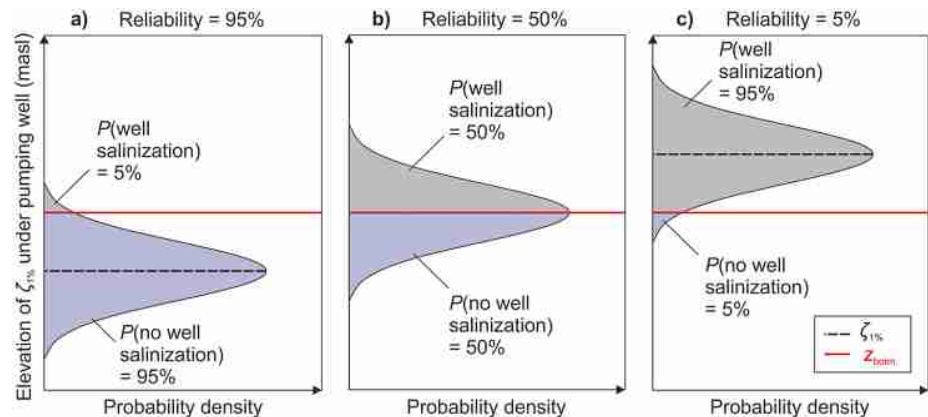

Figure 6. Probability densities associated with the steady-state elevation of the 1% seawater salinity contour ($\zeta_{1\%}$), after (a) risk-averse, (b) risk-neutral, and (c) risk-tolerant optimizations (modified from White et al., 2018). Panels (a–c) represent reliability levels of 95%, 50% and 5%, respectively, corresponding to respective risks of well salinization of 5%, 50%, and 95%. The red line indicates well bottom elevation (z_{botm}).
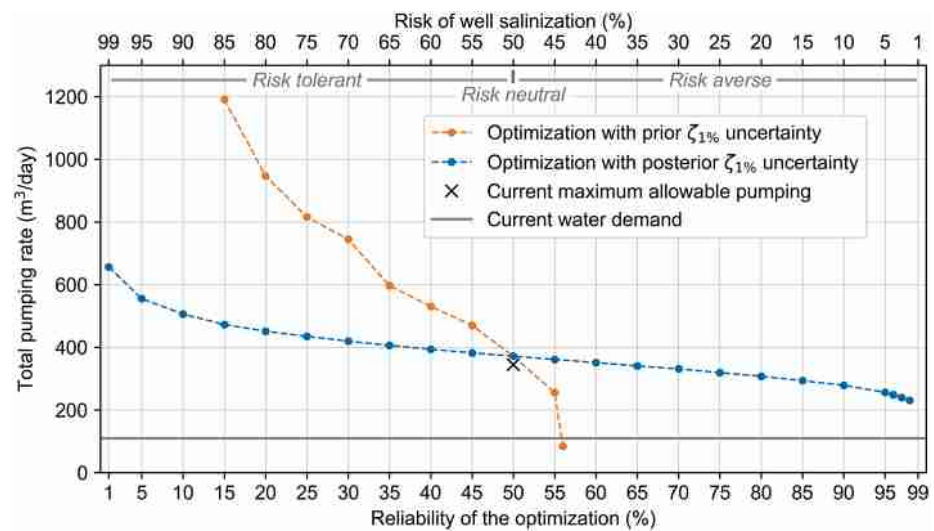
Figure 7. Total pumping rate in the well field versus reliability level (bottom axis) or risk of well salinization (top axis), for optimizations conducted using prior $\zeta_{1\%}$ (constraint) uncertainty (orange curve) or posterior $\zeta_{1\%}$ uncertainty (blue curve). The current maximum allowable pumping in the well field and current water demand are shown, as well as risk-tolerant, neutral, and averse areas.

slightly with decision variable values (indicative of model nonlinearities). As a side analysis, the optimizations were also run once with the posterior parameter set and with prior $\zeta_{1\%}$ standard deviations, to examine the tradeoff between pumping and risk that would have been obtained if no observations had been available to condition parameter estimation.

4. Results

Solving the optimization problem for the 23 risk values required approximately 5,900 model simulations (233 and 310 simulations for non-risk-neutral optimizations with convergence at 3 and 4 SLP iterations, respectively). Using 72 cores at 2.3 GHz, this process took 37.5 hr. The results of optimization under uncertainty were explored by analyzing curves of the maximum pumping in the well field (i.e., the management objective function), maximum pumping rates at individual wells (i.e., the decision variables), and $\zeta_{1\%}$ values (i.e., the constraints) versus reliability.

4.1. Total Pumping in the Well Field

As expected, the total pumping rate in the well field decreased as aversion to risk increased (Figure 7, blue curve) and the tradeoff between the total pumping rate and risk could be quantified. For example, reducing the risk of salinization from 50% (risk-neutral scenario) to 5% (highly risk-averse scenario) required a 115 m³/day decrease in total pumping. For all risk stances, the total pumping in the well field remained far above the current water demand, estimated at 110 m³/day. Overall, the total pumping rates were of the same order of magnitude as the maximum pumping rate currently allowed in the well field, obtained from advective-dispersive-based VD models. The optimization problem was infeasible for a reliability level of 99%.

Running the optimizations using prior $\zeta_{1\%}$ standard deviations (Figure 7, orange curve) resulted in a much steeper curve of total pumping versus reliability. For example, reducing the risk of well salinization from 50% to 45% required a 116 m³/day decrease in pumping with prior $\zeta_{1\%}$ uncertainties, but only a 10 m³/day decrease in pumping with posterior $\zeta_{1\%}$ uncertainties. This steeper curve can be explained by the fact that prior $\zeta_{1\%}$ constraint uncertainties were much higher than posterior $\zeta_{1\%}$ constraint uncertainties (on average 43 and 5 m, respectively). When using prior $\zeta_{1\%}$ uncertainties, the lowest risk of well salinization that could be achieved was 44%, for a total pumping rate of 84 m³/day, since the optimization became infeasible for reliability levels above 56%. In comparison, when using posterior $\zeta_{1\%}$ uncertainties, the lowest risk of well salinization that could be achieved was 2%, for
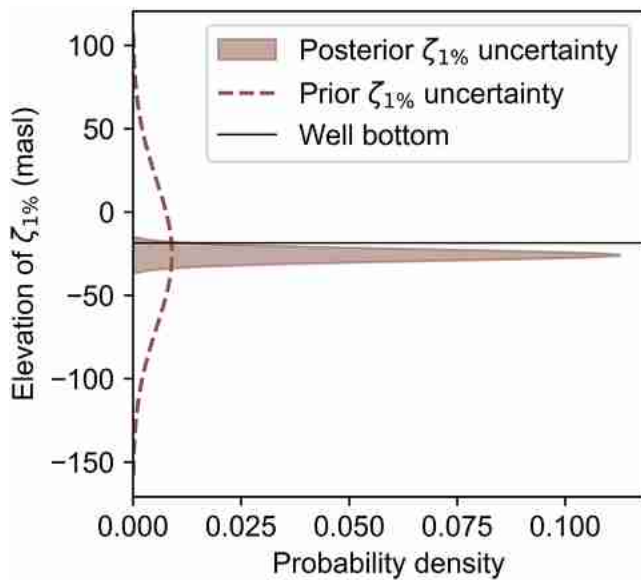
a pumping rate of 231 m³/day. The probability densities associated with the $\zeta_{1\%}$ values at the end of these optimizations are shown Figure 8.

4.2. Pumping Rates at Individual Wells

Individual pumping rates decreased as aversion to risk increased (Figure 9), and the allocation of the total pumping amongst individual wells was obtained for each reliability level. The tradeoff between pumping and risk could be quantified for any well. For instance, if a pumping scenario with a 95% reliability was selected, then increasing the pumping rate by 10 m³/day would increase the risk of salinization by 15% at well no. 1 (blue curve) versus 85% at well no. 4 (near-horizontal red curve). Also, achieving highly risk-averse stances required reducing the pumping rate in well no. 7 to close to zero. Overall, the individual pumping rates were on the same order of magnitude as those currently applied in the field, but with different allocations.

As aversion to risk increased, under each pumping well, progressively more of the probability distribution of $\zeta_{1\%}$ was located below the well bottom elevation at the new steady state (Figure 10). In parallel, the interface simulated by SWI2 (ζ_{cell}, Equation 4) approached its initial elevation and the transition zone width decreased. For the high pumping rates applied at low reliability levels, while simulated ζ_{cell} values remained well below sea level, the $\zeta_{1\%}$ values obtained through postprocessing could have portions of their probability distribution (or even their mean value) located above sea level, which is a limitation of the postprocessing approach. However, adopting such

Figure 8. Prior and posterior constraint uncertainty associated with the 1% seawater salinity contour ($\zeta_{1\%}$) under well no. 6, for the lowest-risk optimization that was achievable in each case (44% and 2% risks of well salinization, respectively).

risk-tolerant stances is not advisable. Finally, the computed values for the $\zeta_{1\%}$ uncertainty varied between optimizations (Figure 10), which could be attributed to model nonlinearity. These variations increased in magnitude when conducting optimization using the higher, prior $\zeta_{1\%}$ uncertainties, which was responsible for the irregular aspect of the total pumping versus risk curve (Figure 7, orange curve). The steady-state freshwater lens obtained with the optimized pumping rates was analyzed using maps and cross-sections. In the study area, higher pumping rates generated more significant upconing but also a contraction of the lens farther away from the pumping wells (Figure 11).
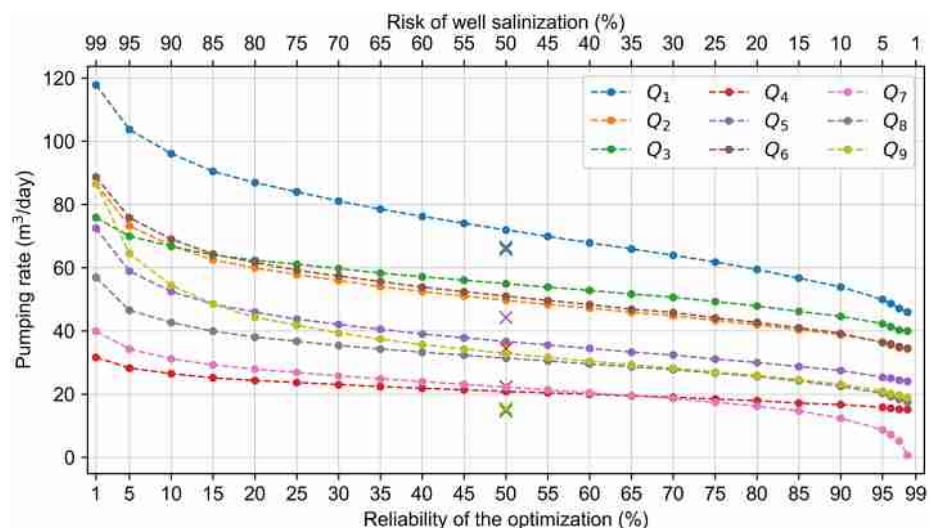

Figure 9. Pumping rates at individual wells (Q_i) versus reliability level (bottom axis) or risk of well salinization (top axis). The maximum allowable pumping rates currently implemented at each well are represented by crosses.
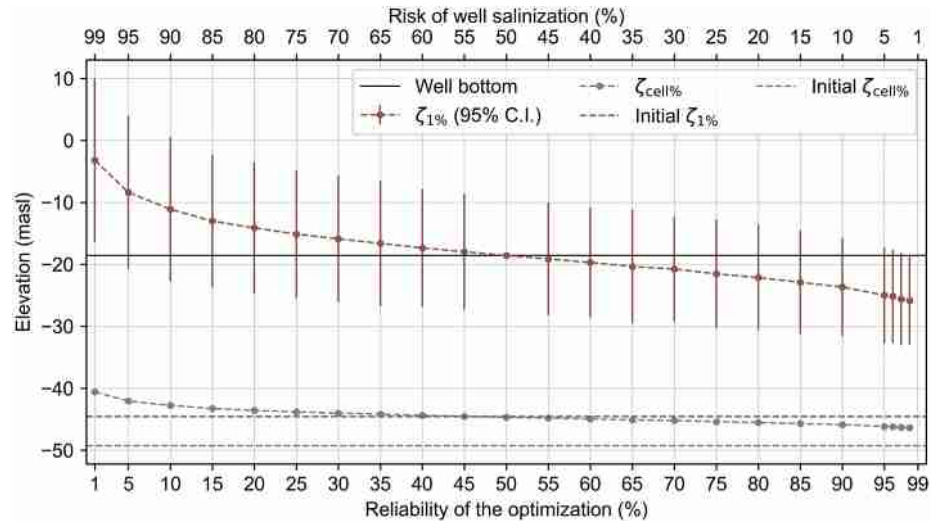
Figure 10. Elevation of the 1% seawater salinity contour ($\zeta_{1\%}$) and its 95% confidence interval versus reliability level, at well no. 6. The elevation of the interface simulated by SWI2 is shown (ζ_{cell}), with the well bottom elevation (z_{botm}) and initial $\zeta_{1\%}$ and ζ_{cell} values. PESTPP-OPT does not compute constraint uncertainty for risk-neutral optimizations.

5. Discussion

5.1. Pumping Optimization Under Uncertainty

Comparing the maximum allowable pumping rate for different risk stances to the water demand allowed for an examination of the capacity of the well field to satisfy demand while maintaining low levels of risk. In the study area, the well network had the capacity to satisfy the water demand even for the most risk-averse stances (Figure 7). Adopting a highly risk-averse pumping scenario, which was strongly advisable given the consequences of well salinization (Section 3.2.1), was therefore straightforward. Had the water demand intersected the curve in Figure 7, managers could choose to satisfy the water demand at a higher risk of well salinization, or to maintain a low level of risk in the current well network but find supplementary sources of water. Describing not only the probability of well salinization but its consequences, in terms of cost or multiple criteria (e.g., broader economic, societal, environmental impacts) could further support decision-making in these cases. Instead of presenting
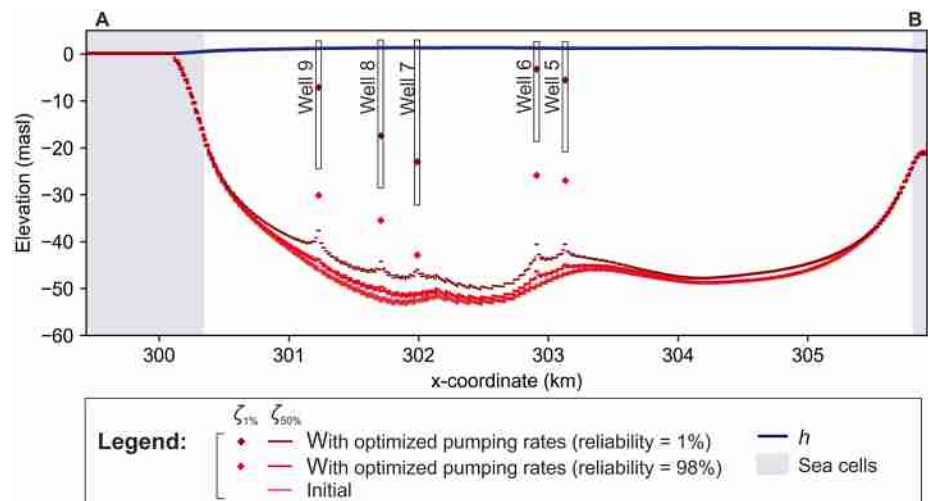

Figure 11. Cross-section of the freshwater lens, delimited by the freshwater head (h) and the 50% seawater salinity contour ($\zeta_{50\%}$), at steady state without pumping and with optimized pumping rates obtained with reliability levels of 98% and 1%. The location of the transect is shown Figure 2. The elevation of the steady-state 1% seawater salinity contour ($\zeta_{1\%}$) is calculated at pumping well locations. $\zeta_{1\%}$ is only equal to well bottom elevation for a reliability level of 50%.

water managers with a unique, final pumping scenario, they are encouraged to choose the final scenario themselves depending on their desired reliability level, or tolerated risk of failure. This is a strong advantage in terms of decision-support, since direct involvement in the decision-making process can lead to a higher adherence. The optimizations further determined how pumping should be allocated within the well field. Analyzing how individual pumping rates varied as a function of risk helped identify at which wells the pumping rate could be increased while maintaining a low risk of salinization, versus wells that were more vulnerable to salinization (e.g., wells no. 1 and 4, respectively, Figure 9).

After parameter estimation, during which constraint uncertainty was significantly reduced, the cost of reducing risk was smaller (i.e., reducing the risk of well salinization could be achieved for smaller reductions in the total pumping rate). Optimal pumping scenarios could also be determined for lower levels of risk (Figure 7). Conducting parameter estimation was therefore essential to improve the results of pumping optimization under uncertainty. It should be noted that the constraint uncertainty decreased significantly because the observations in the calibration data set contained substantial information related to the parameters influencing the $\zeta_{1\%}$ constraint values (Coulon et al., 2021). The results of pumping optimization under uncertainty using the higher constraint uncertainties were affected by higher model nonlinearity, which should be further explored.

5.2. Sharp-Interface Approach for Upconing Problems

The limitations of SI numerical upconing remain largely unexplored. Bakker et al. (2013) found that SWI2 yielded similar results to SEAWAT for a transient upconing simulation, and Reilly and Goodman (1987) found that their steady-state SI numerical model yielded results similar to the advective-dispersive-based SUTRA model (Voss, 1984) for pumping rates below a maximum permissible discharge calculated from sharp-interface theory. During saltwater upconing, the salt concentration distribution is a result of hydraulically-driven (i.e., forced) convection, where pumping-induced head gradients lead to a convergence of flowlines from different depths and salinities to the well (de Louw et al., 2013), density-driven (i.e., free) convection, and hydrodynamic dispersion (Jakovovic et al., 2011; Simmons et al., 2001). Three-dimensional advective-dispersive transport takes place along all flowlines converging to the well, including those from above and below the interface. SWI2 cannot fully reproduce forced vertical or free convection, since it adopts the Dupuit approximation in each zone of differing density (and a single model layer was used to discretize the aquifer – Section 3.1) and it does not account for hydrodynamic dispersion (Bakker et al., 2013). Considering the high hydraulic conductivity of the aquifer and the low pumping rates (resulting in a maximum drawdown of 0.8 m in the most risk-tolerant scenarios), flow to the well was expected to remain dominantly horizontal, that is, with few flowlines originating from the deeper saltwater zone and crossing salinity contours, therefore the SI approach was considered a reasonable compromise between accuracy and computational effort. However, this approach might not be suitable to simulate upconing in cases with a significant vertical flow component, for example, for high pumping rates or low hydraulic conductivities (de Louw et al., 2013). Comparing SWI2 and an advective-dispersive-based VD model under a wide range of aquifer conditions and well parameters would be of interest, to identify specific limitations of the SWI2 package.

The limitations of the analytical correction for dispersion (Equation 5), used in combination with SWI2, should also be explored. Although it accounts for longitudinal dispersion, which dominates mixing in the transition zone during transient phases of upconing (Jakovovic et al., 2011), the correction neglects transverse dispersion, which dominates mixing in steady-state conditions (Reilly & Goodman, 1987). It also assumes a homogeneous domain, although small-scale variability in aquifer properties can significantly impact solute transport (Sudicky, 1986). When superimposing this solution to analytical SI equations and comparing the results with the SEAWAT model, Pauw et al. (2016) found the approach was limited for high pumping rates causing significant upconing, or for wide initial mixing zones. The $\zeta_{1\%}$ values obtained through this approach depended on α_L and M values, which are uninformed by the interface observations used in parameter estimation. The $\zeta_{1\%}$ values were particularly sensitive to α_L, and Jiao and Post (2019) suggest that determining α_L as a function of solute transport scale may not always apply to regional coastal groundwater models (α_L values on the order of a few meters seem most appropriate).

With a SI approach, well salinization could only be defined indirectly, whereas in advective-dispersive-based VD models, pumped water salinity can be directly used. Not only did this add conceptual uncertainty to the approach, but comparison of model predictions and observations is more complicated since only a documented well salinization event could be used to verify or update the predictions. The well salinization definition used in this study (Section 3.2.1) was more conservative than the saltwater ratio of 0.001 used by Babu et al. (2018), since it was

expected that the salinity of pumped water would increase before the 50% seawater salinity contour reached the well. It was also more conservative than the critical interface rise used by Luedeling et al. (2015), since the rise of the SWI2 interface under pumping wells was always less than 40–60% of the original distance from the well bottom (Figure 10). It was also less than the 2.4% seawater salinity contour used by Pauw et al. (2016), which was based on the drinking water standard for total dissolved solids. Comparing optimization results obtained in an upconing context, using both a SI and an advective-dispersive-based VD approach, would be of interest (similar to the comparison by Kopsiaftis et al. (2019) in a lateral seawater intrusion context).

The optimization under uncertainty neglected several sources of uncertainty, including conceptual (or structural) uncertainty, and scenario uncertainty, that is, the uncertainty in future system stresses. In particular, using a SI approach was a major simplification of mixing processes which could result in high conceptual uncertainty as well as biased $\zeta_{1\%}$ values. The model pairing methodology developed by Doherty and Christensen (2011) could be used to detect and correct the SI model's predictive biases and to quantify its predictive uncertainty, through pairing with an advective-dispersive-based VD model.

Although the SI numerical model faced the above-mentioned challenges, its fast simulation times and numerical stability facilitated a rigorous analysis of parameter estimation and pumping optimization under uncertainty. A total of almost 8,000 simulations were run in less than 50 hr (using parallelized model simulations), which is a very low computational burden compared to advective-dispersive-based VD models. Furthermore, all numerical simulations of physical processes face specific challenges, including advective-dispersive-based VD models. For instance, the accurate representation of mixing processes requires input data such as effective molecular diffusion coefficients, which can be highly uncertain (Jiao & Post, 2019), and the inability to conduct parameter estimation due to long simulation times results in high parametric uncertainty and limits uncertainty quantification altogether. Simulation results may also be biased by numerical dispersion (Gatto et al., 2021; Konikow, 2011; Woods et al., 2003). The computational complexity of these models generally requires the use of surrogate models to conduct optimization, which further increases predictive uncertainty (Ketabchi & Ataie-Ashtiani, 2015).

5.3. Other Limitations

The difference between upconing simulated at the cell and upconing under the well will be non-negligible when cell sizes are of the same order of magnitude as the radius of influence of the wells (Panday et al., 1993). While corrections for cell-to-well drawdown were extensively studied and are easily implemented using the MNW2 package (Konikow et al., 2009), corrections for cell-to-well upconing seem unexplored and Equation 4 was used as a first approximation. This correction was required because MODFLOW-2005 does not have local mesh refinement options, and implementing gradational global mesh refinement near pumping wells produced elongated cells in which numerical instabilities developed with the SWI2 package. Using this correction increased the $\zeta_{1\%}$ conceptual uncertainty. It also introduced a dependence of the $\zeta_{1\%}$ values on the h_{well} values computed by MNW2, and thus calculation of h_{well} will vary with the implemented type of head-loss correction (Konikow et al., 2009).

The optimization was conducted under steady-state conditions because the storage parameters were unconstrained by the steady-state calibration, and therefore remained highly uncertain (Coulon et al., 2021). These parameters have no influence on steady-state $\zeta_{1\%}$ uncertainties, but would likely be significant sources of uncertainty for transient $\zeta_{1\%}$ values. However, for constant boundary conditions, the maximum upconing will occur at the new system equilibrium while in a real-life system with varying stresses, the maximum upconing could occur before the new steady state. Working in a transient framework would allow for the evaluation of the rate of change of the system in response to the pumping scenarios, which may be of interest to decision-makers.

6. Conclusion

Conducting pumping optimization under uncertainty for different reliability levels yielded the maximum amount of freshwater that could be extracted by the well field as a function of risk of well salinization. This allowed for the quantification of the tradeoff between total pumping and risk, and for determination of the ability (or inability) of the well field to meet the water demand while maintaining an acceptable risk of well salinization. The approach also yielded the maximum pumping rates at individual wells, or the allocation of total pumping amongst wells, as a function of risk. This enabled an exploration of which wells could see their pumping rates increased

while maintaining an acceptable risk of salinization. Finally, conducting parameter estimation was found to be beneficial, since reduced constraint uncertainties enabled the identification of pumping scenarios with low risks of salinization, and achieved reductions in risk for smaller reductions in pumping. Overall, the methodology provides groundwater managers with multiple insights for groundwater pumping management, while leaving them with the final decision of which pumping scenario to adopt, depending on their degree of tolerance or averseness toward risk.

This methodology can be applied to freshwater lenses in other island aquifers, to determine a first-order approximation of sustainable yields considering uncertainty. The method for pumping optimization under uncertainty could also be adapted to continental coastal aquifers exposed to lateral seawater intrusion, where the definition of well salinization would differ (e.g., based on the location of the "toe" of the interface, Mantoglou et al., 2004). Remaining questions concern the estimation of conceptual uncertainty and of bias in the outputs of the SI numerical models, and the definition of well salinization. In future work, the uncertainty in climate change and water demand scenarios will be considered and integrated into the optimization approach.

Appendix A: Analytical Correction for Dispersion

The application of the analytical correction for dispersion to the MODFLOW-SWI2 model is briefly summarized. Equation 5 in the main text was derived from Pauw et al. (2016), Equation 6. Upconing under a pumping well is considered as a 1D solute transport problem. The hydrodynamic dispersion taking place around the 50% seawater salinity contour (i.e., the center of the transition zone), following the displacement of a transition zone (with an initial width M) from its initial position, is approximated using the Ogata and Banks (1961) 1D solution for advective-dispersive transport. Using this approach, at any given time t, the concentration of any x-percent seawater salinity $C_{x\%}$ (kg/m^3) can be calculated using Equation A1:

$$C_{x\%}(t) = \frac{C_s}{2} \text{erfc}\left(\frac{\zeta_{x\%}(t) - \zeta_{50\%}(t)}{2\sqrt{b\,M^2 + \alpha_L\,|\zeta_{50\%}(t) - \zeta_{50\%\,\text{init}}|}}\right) \tag{A1}$$

where C_s is the seawater salinity (kg/m^3), erfc is the complementary error function, $\zeta_{x\%}$ is the elevation of the $x\%$ seawater salinity contour (masl), $\zeta_{50\%}$ and $\zeta_{50\%\,\text{init}}$ are the elevations of the 50% seawater salinity contours (i.e., the advective front) at time t and the initial state, respectively (masl), α_L is the longitudinal dispersivity (m), M is the initial width of the transition zone (m), defined as the 95% confidence interval around the 50% seawater salinity contour (i.e., $\pm$ 2 standard deviations). This 95% confidence interval corresponds to the difference between the 2.4% and 98% seawater salinity contours ($\zeta_{2.4\%}$ and $\zeta_{98\%}$, respectively), or twice the difference between the 2.4% and the 50% seawater salinity contours, assuming a Gaussian distribution of concentrations:

$$M = \zeta_{2.4\%} - \zeta_{98\%} = 2\,(\zeta_{2.4\%} - \zeta_{50\%}) \tag{A2}$$

In Equation A1, b is a constant whose formulation depends on the definition of the transition zone width M (Pauw et al., 2016, Equation S14). For a transition zone width defined as in Equation A2, b is:

$$b = \left(\frac{1}{4\,\text{erfc}^{-1}\left(2\frac{C_{2.4\%}}{C_s}\right)}\right)^2 \tag{A3}$$

where $C_{2.4\%}$ is the concentration corresponding to 2.4% seawater (i.e., $0.024 \cdot C_s$). Equation A3 corresponds to Equation 6 in the main text.

Equation A1 corresponds to a rearranged form of Pauw et al. (2016), Equation S16, in which Equation S15 was inserted. For an initially null transition zone width ($M = 0$), Equation A1 is similar to the original Ogata and Banks (1961) solution, while for an initially non-null transition zone width, the term $b\,M^2$ represents the "*width of the mixing zone in the form of the equivalent traveled distance of the interface*" (Pauw et al., 2016). Equation A1 is similar to Equation 16 of Schmorak and Mercado (1969), who defined the width of the transition zone as the 68% confidence interval around the 50% seawater salinity contour (i.e., ± 1 standard deviation). As shown in

Equation A1, the concentration distribution in the transition zone depends on the total distance traveled by the 50% seawater salinity contour from its initial position, independent of direction ($|\zeta_{50\%} - \zeta_{50\% \text{ init}}|$).

The sharp interface simulated by MODFLOW-SWI2, ζ_{SWI2}, corresponds to the elevation of the 50% seawater salinity contour (masl). Therefore, rewriting $\zeta_{50\%}$ as ζ_{SWI2}, and rearranging Equation A1, the elevation of any x-percent seawater salinity contour $\zeta_{x\%}$ (masl) can be calculated at any time t using:

$$\zeta_{x\%}(t) = \zeta_{\text{SWI2}}(t) + 2\sqrt{b\,M^2 + \alpha_{\text{L}}|\zeta_{\text{SWI2}}(t) - \zeta_{\text{SWI2 init}}|}\ \text{erfc}^{-1}\left(2\frac{C_{x\%}}{C_{\text{s}}}\right) \tag{A4}$$

Equation A4 is similar to Equation S16 of Pauw et al. (2016). Equation 5 in the main text corresponds to Equation A4 applied to the 1% seawater salinity contour.

Data Availability Statement

Version 1.12.00 of MODFLOW-2005, used for simulations of groundwater flow, is available at https://www.usgs.gov/software/modflow-2005-usgs-three-dimensional-finite-difference-ground-water-model. The PEST_HP software used for parameter estimation is available at https://pesthomepage.org/programs (version 16.11 was used). The PESTPP-OPT software used for pumping optimization is available at https://www.usgs.gov/software/pest-software-suite-parameter-estimation-uncertainty-analysis-management-optimization-and (version 5.1.2 was used, the source code is available on https://github.com/usgs/pestpp). The files associated with the parameter estimation are available as part of the Supplementary data of Coulon et al. (2021), they are available on GitHub at https://github.com/Cecile-A-C/swi2-magdalen-islands and are archived at https://doi.org/10.5281/zenodo.6774214 (version v1.0.0, MIT license). The input and output files of the pumping optimizations, and the Python scripts used for postprocessing output files and for generating figures, are available on GitHub at https://github.com/Cecile-A-C/swi2-optimization and are archived at https://doi.org/10.5281/zenodo.6458507 (version v1.0.0, MIT license).

References

Babu, R., Park, N., Yoon, S., & Kula, T. (2018). Sharp interface approach for regional and well scale modeling of small island freshwater lens: Tongatapu island. *Water*, *10*(11), 1636. https://doi.org/10.3390/w10111636

Bakker, M., Schaars, F., Hughes, J. D., Langevin, C. D., & Dausman, A. M. (2013). *Documentation of the seawater intrusion (SWI2) package for MODFLOW* (Vol. 6). US Geological Survey Techniques and Methods.

Bear, J., & Cheng, A. H.-D. (2010). Optimization, inverse, and management tools. In *Modeling groundwater flow and contaminant transport* (pp. 693–756). Springer. https://doi.org/10.1007/978-1-4020-6682-5_11

Bear, J., & Todd, D. K. (1960). *The transition zone between fresh and salt waters in coastal aquifers* (p. 156). University of California.

Bower, J., Motz, L., & Durden, D. (1999). Analytical solution for determining the critical condition of saltwater upconing in a leaky artesian aquifer. *Journal of Hydrology*, *221*(1–2), 43–54. https://doi.org/10.1016/s0022-1694(99)00078-5

Brisebois, D. (1981). *Lithostratigraphie des strates permo-carboniferes, de l'archipel des Iles de la Madeleine* (Rep. 2550016882). Direction générale des énergies conventionnelles.

Charbeneau, R. J. (1995). Contribution to discussion of "A density-dependent flow and transport analysis of the effects of groundwater development in a freshwater lens of limited areal extent: The Geneva area (Florida, USA) case study by Panday et al. (1993)". *Journal of Contaminant Hydrology*, *18*(4), 335–337. https://doi.org/10.1016/0169-7722(94)00053-k

Coulon, C., Pryet, A., Lemieux, J.-M., Yrro, B. J. F., Bouchedda, A., Gloaguen, E., et al. (2021). A framework for parameter estimation using sharp-interface seawater intrusion models. *Journal of Hydrology*, *600*, 126509. https://doi.org/10.1016/j.jhydrol.2021.126509

Dagan, G. (1995). Contribution to discussion of "A density-dependent flow and transport analysis of the effects of groundwater development in a freshwater lens of limited areal extent: The Geneva area (Florida, USA) case study, by Panday et al. (1993)". *Journal of Contaminant Hydrology*, *18*(4), 332–334. https://doi.org/10.1016/0169-7722(94)00052-j

Dantzig, G. B., Orden, A., & Wolfe, P. (1955). The generalized simplex method for minimizing a linear form under linear inequality restraints. *Pacific Journal of Mathematics*, *5*(2), 183–195. https://doi.org/10.2140/pjm.1955.5.183

de Louw, P. G. B., Vandenbohede, A., Werner, A. D., & Oude Essink, G. H. P. (2013). Natural saltwater upconing by preferential groundwater discharge through boils. *Journal of Hydrology*, *490*, 74–87. https://doi.org/10.1016/j.jhydrol.2013.03.025

Doherty, J. (2003). Ground water model calibration using pilot points and regularization. *Ground Water*, *41*(2), 170–177. https://doi.org/10.1111/j.1745-6584.2003.tb02580.x

Doherty, J. (2004). *Pest: Model-independent parameter estimation user manual* (p. 393). Watermark Numerical Computing.

Doherty, J. (2020). *PEST_HP, PEST for highly parallelized computing environments*. Watermark Numerical Computing.

Doherty, J., & Christensen, S. (2011). Use of paired simple and complex models to reduce predictive bias and quantify uncertainty. *Water Resources Research*, *47*, W12534. https://doi.org/10.1029/2011WR010763

Frind, E. O., & Germain, D. (1986). Simulation of contaminant plumes with large dispersive contrast: Evaluation of alternating direction Galerkin models. *Water Resources Research*, *22*(13), 1857–1873. https://doi.org/10.1029/WR022i013p01857

Gatto, B., Paniconi, C., Salandin, P., & Camporese, M. (2021). Numerical dispersion of solute transport in an integrated surface–subsurface hydrological model. *Advances in Water Resources*, *158*, 104060. https://doi.org/10.1016/j.advwatres.2021.104060

Harbaugh, A. W. (2005). *MODFLOW-2005, the US geological survey modular ground-water model: The ground-water flow process*. US Department of the Interior, US Geological Survey.

Horne, A., Szemis, J. M., Kaur, S., Webb, J. A., Stewardson, M. J., Costa, A., & Boland, N. (2016). Optimization tools for environmental water decisions: A review of strengths, weaknesses, and opportunities to improve adoption. *Environmental Modelling & Software*, *84*, 326–338. https://doi.org/10.1016/j.envsoft.2016.06.028

Izuka, S. K., Rotzoll, K., & Nishikawa, T. (2021). *Volcanic Aquifers of Hawai'i—Construction and calibration of numerical models for assessing groundwater availability on Kaua'i, O'ahu, and Maui* (Rep. 2328-0328). US Geological Survey.

Jakovovic, D., Werner, A. D., & Simmons, C. T. (2011). Numerical modelling of saltwater up-coning: Comparison with experimental laboratory observations. *Journal of Hydrology*, *402*(3–4), 261–273. https://doi.org/10.1016/j.jhydrol.2011.03.021

Jiao, J., & Post, V. (2019). *Coastal hydrogeology*. Cambridge University Press.

Ketabchi, H., & Ataie-Ashtiani, B. (2015). Review: Coastal groundwater optimization—Advances, challenges, and practical solutions. *Hydrogeology Journal*, *23*(6), 1129–1154. https://doi.org/10.1007/s10040-015-1254-1

Konikow, L. F. (2011). The secret to successful solute-transport modeling. *Ground Water*, *49*(2), 144–159. https://doi.org/10.1111/j.1745-6584.2010.00764.x

Konikow, L. F., Hornberger, G. Z., Halford, K. J., & Hanson, R. T. (2009). *Revised multi-node well (MNW2) package for MODFLOW ground-water flow model* (Vol. 67). US Geological Survey Techniques and Methods. https://doi.org/10.3133/tm6a30

Kopsiaftis, G., Christelis, V., & Mantoglou, A. (2019). Comparison of sharp interface to variable density models in pumping optimisation of coastal aquifers. *Water Resources Management*, *33*(4), 1397–1409. https://doi.org/10.1007/s11269-019-2194-7

Lal, A., & Datta, B. (2019). Multi-objective groundwater management strategy under uncertainties for sustainable control of saltwater intrusion: Solution for an island country in the South Pacific. *Journal of Environmental Management*, *234*, 115–130. https://doi.org/10.1016/j.jenvman.2018.12.054

Langevin, C. D., Thorne, D. T., Jr., Dausman, A. M., Sukop, M. C., & Guo, W. (2008). *SEAWAT version 4: A computer program for simulation of multi-species solute and heat transport* (Rep. 2328-7055). Geological Survey (US).

Lemieux, J.-M., Germain, A., Tremblay, Y., Gatel, L., Arbour, G., Coulon, C., & Dupuis, C. (2022). *Portrait des ressources en eau souterraine des îles de la Madeleine (Portrait of groundwater resources in the Magdalen Islands)*. Département de géologie et de génie géologique.

Lotti, F., Borsi, F., Guastaldi, E., Barbagli, A., & Basile, P. (2021). Numerically enhanced conceptual modelling (NECoM) applied to the Malta mean sea level aquifer. *Hydrogeology Journal*, *29*(4), 1517–1537. https://doi.org/10.1007/s10040-021-02330-2

Luedeling, E., Oord, A. L., Kiteme, B., Ogalleh, S., Malesu, M., Shepherd, K. D., & De Leeuw, J. (2015). Fresh groundwater for Wajir—Ex-ante assessment of uncertain benefits for multiple stakeholders in a water supply project in Northern Kenya. *Frontiers in Environmental Science*, *3*, 16. https://doi.org/10.3389/fenvs.2015.00016

Mantoglou, A., Papantoniou, M., & Giannoulopoulos, P. (2004). Management of coastal aquifers based on nonlinear optimization and evolutionary algorithms. *Journal of Hydrology*, *297*(1–4), 209–228. https://doi.org/10.1016/j.jhydrol.2004.04.011

Molson, J. W., & Frind, E. O. (2012). On the use of mean groundwater age, life expectancy and capture probability for defining aquifer vulnerability and time-of-travel zones for source water protection. *Journal of Contaminant Hydrology*, *127*(1–4), 76–87. https://doi.org/10.1016/j.jconhyd.2011.06.001

Mostafaei-Avandari, M., & Ketabchi, H. (2020). Coastal groundwater management by an uncertainty-based parallel decision model. *Journal of Water Resources Planning and Management*, *146*(6), 04020036. https://doi.org/10.1061/(ASCE)WR.1943-5452.0001227

Neuman, S. P. (1990). Universal scaling of hydraulic conductivities and dispersivities in geologic media. *Water Resources Research*, *26*(8), 1749–1758. https://doi.org/10.1029/WR026i008p01749

Ogata, A., & Banks, R. B. (1961). A solution of the differential equation of longitudinal dispersion in porous media. *US Government Printing Office*.

Panday, S., Huyakorn, P. S., Robertson, J. B., & McGurk, B. (1993). A density-dependent flow and transport analysis of the effects of groundwater development in a freshwater lens of limited areal extent: The Geneva area (Florida, USA) case study. *Journal of Contaminant Hydrology*, *12*(4), 329–354. https://doi.org/10.1016/0169-7722(93)90004-c

Pauw, P. S., van der Zee, S. E., Leijnse, A., & Oude Essink, G. H. (2016). Saltwater upconing due to cyclic pumping by horizontal wells in freshwater lenses. *Ground Water*, *54*(4), 521–531. https://doi.org/10.1111/gwat.12382

Rajabi, M. M., & Ketabchi, H. (2017). Uncertainty-based simulation-optimization using Gaussian process emulation: Application to coastal groundwater management. *Journal of Hydrology*, *555*, 518–534. https://doi.org/10.1016/j.jhydrol.2017.10.041

Reilly, T., & Goodman, A. (1987). Analysis of saltwater upconing beneath a pumping well. *Journal of Hydrology*, *89*(3–4), 169–204. https://doi.org/10.1016/0022-1694(87)90179-x

Schmorak, S., & Mercado, A. (1969). Upconing of fresh water—Sea water interface below pumping wells, field study. *Water Resources Research*, *5*(6), 1290–1311. https://doi.org/10.1029/WR005i006p01290

Shuler, C. K., & Mariner, K. E. (2020). Collaborative groundwater modeling: Open-source, cloud-based, applied science at a small-island water utility scale. *Environmental Modelling & Software*, *127*, 104693. https://doi.org/10.1016/j.envsoft.2020.104693

Simmons, C. T., Fenstemaker, T. R., & Sharp, J. M., Jr. (2001). Variable-density groundwater flow and solute transport in heterogeneous porous media: Approaches, resolutions and future challenges. *Journal of Contaminant Hydrology*, *52*(1–4), 245–275. https://doi.org/10.1016/s0169-7722(01)00160-7

Sudicky, E. A. (1986). A natural gradient experiment on solute transport in a sand aquifer: Spatial variability of hydraulic conductivity and its role in the dispersion process. *Water Resources Research*, *22*(13), 2069–2082. https://doi.org/10.1029/WR022i013p02069

Thiem, G. (1906). *Hydrologische Methoden: Dissertation zur Erlangung der Würde eines Doktor-Ingenieurs durch die Königliche Technische Hochschule zu Stuttgart*. JM Gebhardt's Verlag.

Voss, C. I. (1984). A finite-element simulation model for saturated-unsaturated, fluid-density-dependent ground-water flow with energy transport or chemically-reactive single-species solute transport. *Water Resources Investigation Report*, *84*, 4369

Wagner, B. J., & Gorelick, S. M. (1987). Optimal groundwater quality management under parameter uncertainty. *Water Resources Research*, *23*(7), 1162–1174.

White, J. T., Fienen, M. N., Barlow, P. M., & Welter, D. E. (2018). A tool for efficient, model-independent management optimization under uncertainty. *Environmental Modelling & Software*, *100*, 213–221. https://doi.org/10.1016/j.envsoft.2017.11.019

White, J. T., Fienen, M. N., & Doherty, J. E. (2016). A python framework for environmental model uncertainty analysis. *Environmental Modelling & Software*, *85*, 217–228. https://doi.org/10.1016/j.envsoft.2016.08.017

Wirojanagud, P., & Charbeneau, R. J. (1985). Saltwater upconing in unconfined aquifers. *Journal of Hydraulic Engineering*, *111*(3), 417–434. https://doi.org/10.1061/(ASCE)0733-9429(1985)111:3(417)

Woods, J. A., Teubner, M. D., Simmons, C. T., & Narayan, K. A. (2003). Numerical error in groundwater flow and solute transport simulation. *Water Resources Research*, *39*(6), 1158. https://doi.org/10.1029/2001WR000586

World Health Organization (WHO). (2003). *Chloride in Drinking-water. Background document for preparation of WHO Guidelines for drinking-water quality*. World Health Organization.

Xu, M., & Eckstein, Y. (1995). Use of weighted least-squares method in evaluation of the relationship between dispersivity and field scale. *Ground Water*, *33*(6), 905–908. https://doi.org/10.1111/j.1745-6584.1995.tb00035.x